Proteome profiling of formalin-fixed, paraffin-embedded lung adenocarcinoma tissues using a tandem mass tag-based quantitative proteomics approach

QI XIE[1], DAN WANG[2], XIAO LUO[3], ZHEN LI[1], AIXIA HU[1], HUI YANG[4], JINXING TANG[4], PEIYU GAO[4], TINGYI SUN[1] and LINGFEI KONG[1]

Departments of [1]Pathology and [2]Neorology; [3]International Medical Center; [4]Department of Thoracic Surgery, Henan Provincial People's Hospital, People's Hospital of Zhengzhou University, People's Hospital of Henan University, Zhengzhou, Henan 450003, P.R China

Received March 29, 2021; Accepted June 22, 2021

DOI: 10.3892/ol.2021.12967

Abstract. Over the past few decades, increasing efforts have been made to improve the understanding of, and treatment options for, lung adenocarcinoma (LUAD). However, considering the heterogeneity of LUAD, precise proteomics-based characterization at the molecular level is an urgent clinical requirement for effective treatment. Formalin-fixed, paraffin-embedded (FFPE) tissue is a good option as the working tool for proteomics studies. The present study aimed to obtain a global protein profile using LUAD FFPE tissue samples. Using a quantitative proteomics approach, the study revealed that 360 proteins were significantly more highly expressed in LUAD than in adjacent nontumor lung tissues. Also, 19 differentially expressed membrane proteins were found to be primarily responsible for immune processes. Epidermal growth factor (EGF)-like domain and laminin EGF domain showed markedly different expression levels between cancer tissues and tumor-adjacent normal tissues. Furthermore, Gene Ontology functional enrichment analysis showed that significantly upregulated proteins were associated with the endoplasmic reticulum lumen, protein disulfide isomerase activity, vitamin binding, cell cycle G_1/S phase transition, to name but a few. Also, numerous kinases and post-translational modification enzymes were significantly upregulated across all eight LUAD samples compared with paracarcinoma tissues. Proteomics analysis revealed that AAA domain containing 3A (ATAD3a), a member of the ATPase family, was highly expressed in LUAD tissues, which was supported by immunohistochemical analysis. Furthermore, the study confirmed that ATAD3a enhanced the cisplatin sensitivity of LUAD cells. Collectively, the findings of the present study provide new potential candidate targets in patients with LUAD, and may aid auxiliary LUAD diagnosis and surveillance in a noninvasive manner.

Correspondence to: Professor Tingyi Sun or Professor Lingfei Kong, Department of Pathology, Henan Provincial People's Hospital, People's Hospital of Zhengzhou University, People's Hospital of Henan University, 7 Weiwu Road, Jinshui, Zhengzhou, Henan 450003, P.R. China
E-mail: suntingyi96@126.com
E-mail: blkklf@163.com

Key words: formalin-fixed, paraffin-embedded tissues, tandem mass tag-based quantitative proteomics, lung adenocarcinoma, novel biomarkers, bioinformatics analysis

Introduction

Lung cancer is one of the most frequently occurring malignant tumors in women and men. Non-small cell lung cancer (NSCLC) is a major type of lung cancer, accounting for four fifths of lung cancer cases worldwide, and can be further divided into lung adenocarcinoma (LUAD) and squamous cell carcinoma (1). LUAD is more likely to occur in women and nonsmokers, and patients are more prone to metastasis. The primary challenges in LUAD therapy are diagnosis at the intermediate or advanced stages, as well as tumor heterogeneity, since high genetic heterogeneity exists between different LUAD cells. Therefore, increasing efforts have been made to identify different 'driver mutations,' primarily comprising the epidermal growth factor receptor (EGFR), anaplastic lymphoma kinase, ROS proto-oncogene 1, receptor tyrosine kinase and KRAS (2,3). KRAS mutations are associated with the expression of programmed cell death 1 ligand 1, which suggests that it may predict immunotherapeutic benefits. However, none of the patients in the present study exhibited KRAS mutations.

Understanding cellular heterogeneity is important in precision oncology. Proteomics research, the study of all the proteins in a biological system, has provided a crucial understanding of cellular heterogeneity, and major advances in proteomics have been applied to clinical usage and personalized therapy (4-6). The use of formalin-fixed, paraffin-embedded (FFPE) samples represents the gold standard for tissue preservation, and is the most common method for preserving tissue morphology and the proteome of clinical specimens (7). In cancer research, FFPE samples

have attracted increasing attention as an alternative to fresh tissues (8-10). Mass spectrometry (MS)-based proteomics has become a formal research tool for the study of FFPE human and animal tissue samples (11,12).

In the present study, 'FFPE proteomics' was adopted for proteomics research on LUAD tissues and matched-adjacent nontumor tissues. Tandem mass tags (TMTs), in combination with high-resolution LC-MS/MS analysis, were used to identify >5,800 proteins. AAA domain containing 3A (ATAD3a), a member of the ATPase family, plays a crucial role in metabolic activity and has been shown to be a novel therapeutic target (13). However, the role and mechanism of ATAD3a in LUAD remain unclear. The present study further confirmed that ATAD3a downregulation enhanced the sensitivity of LUAD cells to cisplatin. Collectively, the results suggested sensitive diagnostic signatures and novel therapeutic targets for LUAD. From the initial screening to treatment decisions through recurrence and monitoring, proteomics plays an important role. The present study aimed to identify similar markers for the presence or prognosis of disease, or targeted proteins that can be found in LUAD through the applied use of proteomics technologies.

Materials and methods

Cell culture. The LUAD cancer cell line (NCI-H292) was cultured in RPMI-1640 supplemented with 10% FBS (both Gibco; Thermo Fisher Scientific, Inc.) and a mixture of 1% penicillin (100 U/ml)/streptomycin (100 μg/ml) (Beijing Solarbio Science & Technology Co., Ltd.). As an alternative to primary cultured lung cells, immortalized normal alveolar epithelial cells (HPAEpi C), as well as the LUAD cancer cell line A549, were cultured in DMEM (Gibco; Thermo Fisher Scientific, Inc.) supplemented with 10% FBS and 1% penicillin/streptomycin. All cell lines were maintained at 37˚C (5% CO_2) in a humidified atmosphere.

Tissue samples. The present study was approved by the Research Ethics Committee of Henan Provincial People's Hospital (HPPH), and written informed consent was obtained from all patients. FFPE LUAD specimens and adjacent nontumor lung tissues were acquired from patients who underwent thoracic surgery at HPPH between May 2019 and February 2020; the basic patient information is presented in Table I. The exclusion criteria were as follows: i) Patients who received chemotherapy or radiotherapy; and ii) patients who possessed other types of tumor. The inclusion criteria were as follows: i) All clinicopathological diagnoses were confirmed by two highly skilled pathologists; ii) none of the patients received any treatments before surgery; iii) no history of other synchronous malignancies; and iv) no death within the perioperative period.

Sample preparation and TMT labeling. The 5 μm-thick FFPE samples were dewaxed for 10 min using xylene at room temperature, and then centrifuged for 10 min at 12,000 x g at room temperature. The supernatant was discarded, and the sediment was rehydrated with a descending ethanol series (absolute, 85, 75% and ddH_2O).

Samples were applied to 5 kD cutoff filters (Agilent Technologies, Inc.) to perform buffer exchange. Then, 5X the sample volume of 50 mm Hepes buffer (pH 7.6) was added to each sample. The filters were subsequently centrifuged for 20 min at 2,000 x g at room temperature and the flow through was discarded. This step was repeated three times to ensure that a complete exchange was achieved. Protein concentrations of the collected samples were subsequently determined with a DC Protein assay (Bio-Rad Laboratories, Inc.). The volume of each sample containing 30 μg protein was adjusted to 120 μl with the addition of 50 mm HEPES (pH 7.6). The samples were subsequently denatured at 99˚C for 5 min. Reduction and alkylation were performed by adding 13 μl of 100 mm dithiothreitol and 20 μl of 100 mm iodoacetamide to each sample. Tryptic digestion was performed overnight at 37˚C (trypsin: Sample ratio, 1:60), followed by TMT labeling, according to the manufacturer's instructions (Thermo Fisher Scientific, Inc.). Following digestion, 5 μl of each sample was taken off and run on a short gradient LC-MS/MS for quality control. The samples were subsequently dissolved in 15 μl of mobile phase A (95% water, 0.1% formic acid) and 1 μl and subjected to LC-MS/MS analysis using a hybrid Q-Exactive mass spectrometer (Thermo Fisher Scientific, Inc.) as described in 2.5.3. To create an internal standard to link the four TMT sets, a pooled internal standard from TIFs was prepared by taking 4 μg from each sample. TIF samples for in-depth analysis were subjected to TMT labeling according to the manufacturer's instructions (Thermo Fisher Scientific, Inc.). The four TMT-labeled sets were desalted and cleaned up by applying them to Strata SCX cartridges, according to the manufacturer's instructions (Phenomenex, https://www.phenomenex.com.cn), followed by lyophilization. The samples were stored at -20˚C until subsequent experimentation.

HPLC fractionation and LC-MS/MS analysis. For each LC-MS analysis, the auto sampler (Ultimate 3000 RSLC System; Thermo Fisher Scientific, Inc.) dispensed 15 μl of mobile phase A (95% water, 5% dimethyl sulfoxide, 0.1% formic acid) into the corresponding well of a 96-well V-bottom polystyrene microtiter plate (Corning, Inc.). When mixed together, the samples was added to the plate by aspirating/dispensing a 10 μl volume 10 times. Subsequently, a 7-μl aliquot was injected into a C18 guard desalting column (Acclaim Pepmap 100, 75 μm x 2 cm, NanoViper; Thermo Fisher Scientific, Inc.). After 5 min with the loading pump at a flow rate of 5 μl·min^{-1}, the 10-port valve switched to analysis mode with the NC pump providing a flow rate of 250 nl·min^{-1} through the guard column. The curved gradient (curve 6 in chromeleon software, Thermo Fisher Scientific, Inc.) was subsequently applied with 3% mobile phase B (95% acetonitrile, 5% water, 0.1% formic acid) increased to 45% mobile phase B over 50 min, followed by a wash with 99% mobile phase B and re-equilibration. The total LC-MS run time was 74 min. A nano EASY-Spray column (Pepmap RSLC, C18, 2 μm bead size, 100 Å, 75 μm internal diameter, 50 cm length; Thermo Fisher Scientific, Inc.) was used on the nano electrospray ionization (NSI) EASY-Spray source (Thermo Fisher Scientific, Inc.) at 60˚C. Online LC-MS was performed using a hybrid Q-Exactive mass spectrometer (Thermo Fisher Scientific, Inc.). FTMS master scans with 70,000 resolution and a mass range of 300-1,700 m/z were followed by data-dependent MS/MS at 35,000 resolution for

Table I. Basic information about the LUAD patients.

Patient no.	Age (years)	Sex	TNM stage
1	66	F	II
4	70	M	III
5	64	F	IV
6	59	F	III
7	69	F	III
9	46	M	IV
10	61	F	III
11	76	M	II

M, male; F, female.

the top five ions by using higher energy collision dissociation (HCD) at 30% normalized collision energy. Precursors were isolated with a 2 m/z window. Automatic gain control targets were 1e6 for MS1 and 1e5 for MS2. Maximum injection times were 100 ms for MS1 and 450 ms for MS2. The entire duty cycle lasted 2.5 sec. Dynamic exclusion was used with 60 sec duration. Precursors with an unassigned charge state or a charge state of 1 were excluded. An underfill ratio of 1% was used. MS/MS data were searched by using Sequest HT of the proteome discoverer 1.4 software platform (Thermo Fisher Scientific, Inc.) against the UniProt protein sequence database (140407) with a 1% peptide false discovery rate (FDR) cut-off. A precursor mass tolerance of 10 p.p.m. and product mass tolerances of 0.02 Da were used. Additional settings were as follows: Trypsin with 1 missed cleavage; IAA on cysteine, TMT on lysine, N-terminal as fixed modification, oxidation of methionine, and phosphorylation of serine, threonine, or tyrosine as variable modifications. Quantitation of TMT 10-plex reporter ions was performed using Proteome Discoverer (Thermo Fisher Scientific, Inc.) on HCD-FTMS tandem mass spectra by using an integration window tolerance of 20 p.p.m. FDR rate was estimated by using percolator (part of PD 1.4). The mass spectrometry proteomics data obtained have been deposited into the ProteomeXchange Consortium2 via the PRIDE partner repository with the dataset identifier, PXD001686.

Protein annotation and functional enrichment. Gene Ontology (GO), protein domain, Kyoto Encyclopedia of Genes and Genomes (KEGG) and subcellular localization annotation was performed using the Database for Annotation, Visualization and Integrated Discovery (https://david.ncifcrf.gov). GO annotation at the proteomics level was carried out using the UniProt-GOA database. InterProScan is based on protein sequence algorithms, and the InterPro homologous domain database annotates the domains of identified proteins. The KEGG Automatic Annotation Server identifies and then annotates proteins, and matches them with corresponding pathways via KEGG mapper. WoLF PSORT software was used to determine the subcellular localization of proteins. For functional enrichment, Fisher's exact test was used to identify significantly differentially expressed proteins between LUAD and adjacent nontumor lung tissues, and $P<0.05$ was considered to indicate a statistically significant difference.

Western blot analysis. Cells were lysed using cell lysis buffer (Abcam). The BCA method was used to examine the concentrations of different protein samples. The protein samples (20 μg/lane) were separated via 12% SDS-PAGE and transferred to PVDF membranes (Bio-Rad Laboratories, Inc.). After incubating with 5% skimmed milk for 1 h at room temperature, the membranes were incubated overnight at 4˚C with the following primary antibodies: β-actin (Abcam; cat. no. ab8226; 1:1,000 dilution) and ATAD3a (Abcam; cat. no. ab112572; 1:1,000 dilution). The bound antibodies were visualized with a horseradish peroxidase-conjugated secondary antibody (Abcam; cat. no. ab6708; 1:1000 dilution, and Abcam; cat. no. ab7090; 1:1,000 dilution) using enhanced chemiluminescence (Clarity Western ECL; Bio-Rad Laboratories, Inc.) and the Ez-Capture MG system (Atto Corp.). Image Lab analysis software (v4.0; Bio-Rad Laboratories, Inc.) was used to analyze the intensities of protein bands.

Reverse transcription-quantitative (RT-q) PCR and transfection. RNA samples were isolated from tissues and cells using TRIzol® (Invitrogen; Thermo Fisher Scientific, Inc.) according to the manufacturer's protocol. To obtain cDNA, RT was conducted using the iScript kit (Bio Rad Laboratories, Inc.) and the TaqMan RT kit (Applied Biosystems; Thermo Fisher Scientific, Inc.) according to the manufacturers' protocol. The amplification of ATAD3 (forward primer, 5'-GCGAGCCACCGAGAAGAT AAG-3' and reverse primer, 5'-TGGACCATCTCATTGATG CGG-3') and GAPDH (forward primer, 5'-GGAGCGAGA TCCCTCCAAAAT-3' and reverse primer, 5'-GGCTGTTGT CATACTTCTCATGG-3') was performed using iQSYBR Green SuperMix (Bio Rad Laboratories, Inc.). The following thermocycling conditions were used for qPCR: 95˚C for 5 min, followed by 40 cycles at 95˚C for 30 sec, 60˚C for 40 sec and 72˚C for 30 sec. The quantification was performed using the $2^{-\Delta\Delta Cq}$ method (1,9).

Transfections were performed using Lipofectamine® 2000 (Invitrogen; Thermo Fisher Scientific, Inc.) according to the manufacturer's instruction. The cancer cells were plated into a 6-well plate at a density of $4x10^5$ cells/well, and were transfected with the negative control (si-NC) or ATAD3a-targeting siRNA (si-ATAD3a). The siRNA sequences are as follows: si-NC, AAGTCGGGTCAAGAGAAGC; and si-ATAD3a, AGAUGGAGCUGAGGCAUAA. Plasmid (1 μg) was transfected into cells using Lipofectamine® 2000 (Invitrogen; Thermo Fisher Scientific, Inc.). Following transfection for 7 h at 37˚C, the culture medium was replaced with fresh complete culture medium. Subsequent experimentation were performed 24 h post-transfection.

Colony formation assay. Cells were seeded into 6-well culture dishes and incubated at 37˚C in a humidified incubator for two weeks. Colonies were fixed with 4% paraformaldehyde for 15 min and stained with 0.1% crystal violet for 15 min at room temperature in 20% ethanol and counted. The colony forming cells were measured at a wavelength of 590 nm, using a microplate reader (Molecular Devices, LLC), and the total

number was counted. The average and formation rates of colony forming cells were measured.

Cell cycle and apoptosis assays. The Cell Cycle Analysis Kit (cat. no. FXP0311-100) and Annexin V/PI apoptosis kit (cat. no. FXP018-100; both Beijing 4A Biotech Co., Ltd.) were used to assess cell cycle distribution and apoptosis, respectively, per the manufacturer's instructions. Cell apoptosis was measured via PI/Annexin V-APC staining and analyzed via flow cytometry. Briefly, cells were harvested and washed with PBS. After staining with PI and Annexin V, cell apoptosis was detected on flow cytometry. Cell cycle was measured via PI staining and analyzed via flow cytometry. Briefly, cells were washed three times with iced PBS and fixed in 70% ethanol overnight at 4˚C. After staining with PI, cell cycle was detected via flow cytometry. Flow cytometric data were analyzed using Kaluza analysis software kaluza C Beckman analysis software (version 2.1, Beckman Coulter, Inc.).

Immunohistochemistry. Tissue sections (3-μm-thick) were fixed with 10% formaldehyde and embedded in paraffin, then they were heated at 60˚C for 2 h, dewaxed for 20 min in xylene twice, and rehydrated in gradient ethanol. Antigen repair was performed in citrate buffer (pH 6.0, 10 mM) in the microwave (95˚C for 15 min), and blocked with 3% H_2O_2 for 15 min at 28˚C. After washing with PBS, the slices were incubated with 5% bovine serum (Gene Tech) to block the nonspecific binding, and the anti-ATAD3a antibody (Abcam; cat. no. ab112572; 1:200 dilution) was incubated overnight at 4˚C. After washing three times, the tissue slices were incubated with horseradish peroxidase coupled double antibody (dilution 1:300; Gene Tech; cat. no. 2017-416029) at room temperature for 30 min, according to the manufacturer's instructions. Tissue sections were immersed in 3,3-o-diamino-benzidine (Gene Tech) for 2 min, stained with hematoxylin, dehydrated and observed under a light microscope (Olympus BX51, x400 magnification).

Statistical analysis. Data analysis was carried out using GraphPad Prism 5 software (GraphPad Software, Inc). The data were analyzed using the Kruskal-Wallis test (non-parametric) followed by a suitable post hoc multiple comparisons test (Tukey's or Bonferroni's) in the event of a significant result. The data were expressed as the mean ± standard deviation. Pearson's correlation analysis was performed to compare pairwise comparisons among all the samples. For functional enrichment, Fisher's exact test was used to assess the differences in expressed proteins between LUAD and adjacent nontumor lung tissues. $P<0.05$ was considered to indicate a statistically significant difference.

Results

Experimental flow graph of quantitative proteomics analysis. The quantitative results of biological repeat samples were examined to determine whether they were statistically consistent. Fig. 1A shows a heat map of the Pearson's correlation coefficients of pairwise comparisons among all the samples. The results showed a positive association among all cancer samples and a negative association between cancerous and normal samples, suggesting that the samples accorded with statistical consistency. Next, to obtain the protein profile of LUAD, cancer tissues and matched-adjacent nontumor tissues from eight FFPE LUAD tissues were selected for proteomics analysis according to strict standards. Tissue specimens from the eight patients with LUAD were successfully analyzed by tandem mass spectrometry combined with LC-MS/MS. Table II showed that mapping table of sample name and labeling reagent. Two parallel TMT-10 PLEX experiments were carried out; every four pairs of LUAD FFPE tissue samples were mixed in each experiment (Fig. 1B).

Table II. Mapping table of sample name and labeling reagent.

Sample name	Labeling reagent	Sample name	Labeling reagent
T1	126	T7	126
NT1	127N	NT7	127N
T4	128N	T9	128N
NT4	128C	NT9	128C
T5	129N	T10	129N
NT5	129C	NT10	129C
T6	130N	T11	130N
NT6	130C	NT11	130C
Mix	131	Mix	131

T, tumor; NT, non-tumor; N, N isotope; C, C isotope.

Identification and quantification of proteins and GO functional annotation analysis of differentially expressed proteins in LUAD. A total of 5,822 proteins were identified, and 5,171 proteins were quantified in eight pairs of LUAD FFPE tissue samples (Fig. 2A). All proteins were identified following false discovery rate correction. To identify differentially expressed proteins, both a fold-change value and a P-value were adopted for comparison, where $P<0.05$ and the fold-change >1.5 or <0.67 were considered as significant. Finally, 360 high-expression proteins and 385 low-expression proteins were obtained in LUAD (Fig. 2B). Functional annotation of differentially expressed proteins was performed by GO analysis. Identified proteins were assigned to specific functions, including biological process (BP), cellular component (CC) and molecular function (MF). BP annotation results indicated that the differentially expressed proteins were primarily involved in 'cellular process', 'single-organism process', 'biological regulation' and 'metabolic process', as well as 'response to stimulus'. According to CC annotation, a large majority of the differentially expressed proteins originated from 'cell', 'organelle', 'membrane' and 'extracellular region' (Fig. 2C). Using MF annotation, it was found that differentially expressed proteins were primarily associated with 'binding', 'structural molecule activity' and 'catalytic activity'.

Subcellular location, protein domain and KEGG enrichment analysis of differentially expressed proteins in LUAD. Subcellular location analysis was conducted to further investigate the differentially expressed proteins associated with LUAD. In the present study, the most differentially expressed proteins were localized to the cytoplasm, extracellular matrix

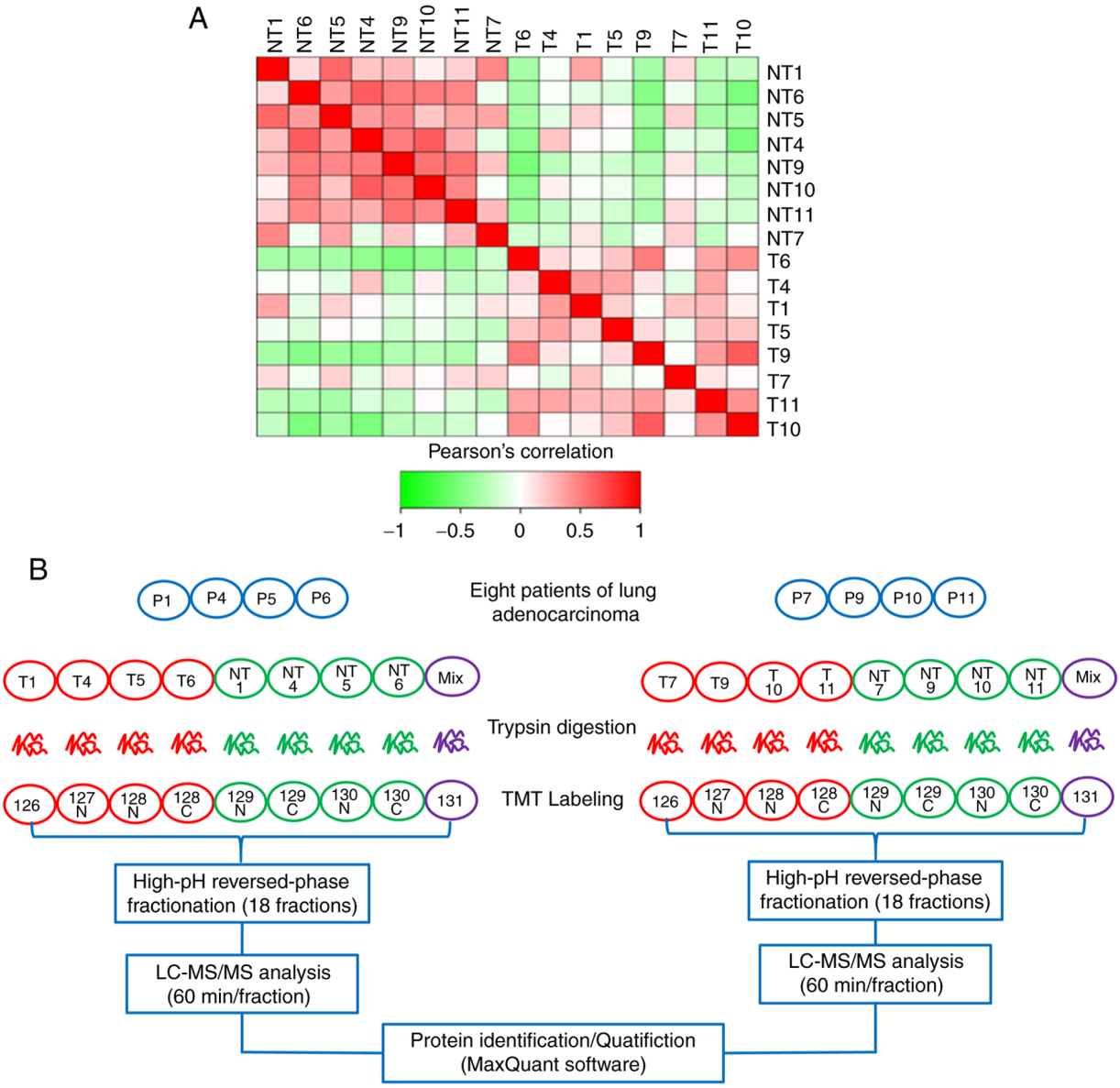

Figure 1. Experimental flow graph of quantitative proteomics analysis. (A) Pearson's correlation values close to 1.0 illustrate a positive correlation, and values close to -1.0 illustrate a negative correlation. (B) Analysis of eight pairs of formalin-fixed, paraffin-embedded cancer tissues and paired normal tumor-adjacent tissues was conducted by dividing the specimens into two groups and two parallel TMT-10 PLEX experiments were performed. Every four pairs of LUAD FFPE tissue samples were mixed in each experiment. T, tumor; N, normal; C, C isotope; P, patients; NT, non-tumor; TMT, tandem mass tag; LC-MS/MS, liquid chromatography and tandem mass-spectrometry.

and nucleus (Fig. 3A). Proteomics was also used to investigate the mechanisms and novel targets of immunotherapy; 19 differentially expressed membrane proteins were primarily involved in immune processes (Table III), indicating that these cell membrane proteins may be potential immunotherapeutic targets.

Through fold enrichment, a number of differentially expressed proteins were enriched in 'EGF-like calcium-binding domain', 'EGF-like domain' and 'laminin EGF domain' (Fig. 3B and Table IV), suggesting that the EGF domain and EGF-like domain play an important role in LUAD. KEGG is a bioinformatics resource for identifying the functions and cells types of organisms (14). KEGG pathway analysis revealed that pathways involved in 'thiamine metabolism' and 'DNA replication' were highly expressed in cancer tissues (Fig. 3C). This was in accordance with the strong proliferative capacity and high mutation rates of cancer cells. The study also showed that 'tight junction', 'PI3K-Akt signaling pathway' and 'nitrogen metabolism' were downregulated in cancer tissues (Fig. 3C). Furthermore, several metabolic pathways, including 'glutamate metabolism' and 'fructose and galactose metabolism', were significantly enriched in cancer tissues (Fig. 3C). Furthermore, enrichment analysis demonstrated that significantly upregulated proteins were associated with the 'endoplasmic reticulum lumen', 'protein disulfide isomerase activity', 'vitamin binding' and 'cell cycle G_1/S phase transition'.

Cluster analysis of GO enrichment of differentially expressed proteins in LUAD. When further performing GO functional enrichment analysis, it was found that 360 high-expression and 385 low-expression proteins in cancer tissues were considerably differently expressed in CC, MF and BP. In

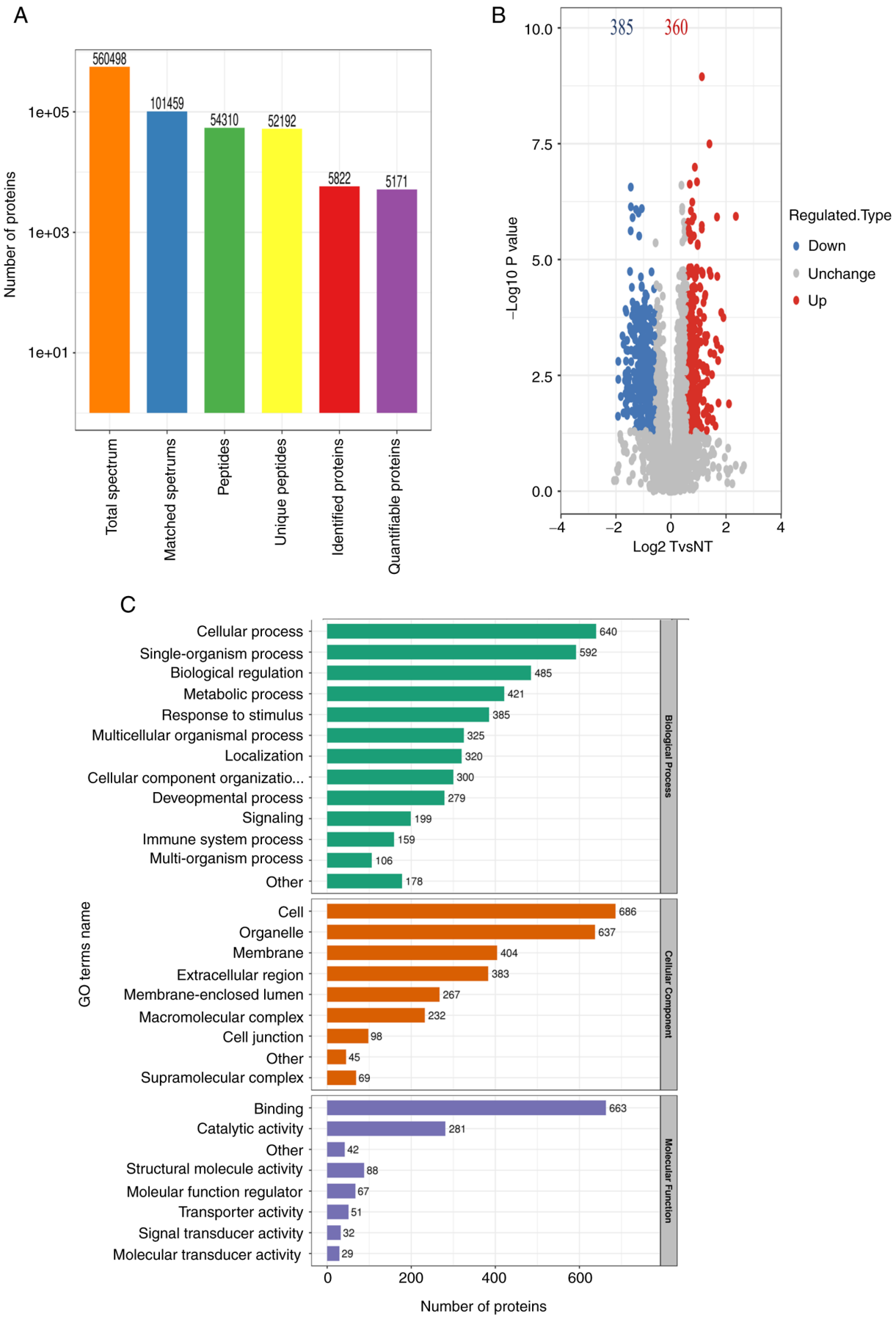

Figure 2. Identification and quantification of proteins and GO functional annotation analysis of differentially expressed proteins in LUAD. (A) Statistics for mass spectrometry-based biological data. (B) Volcano plots of differentially expressed proteins between LUAD and corresponding non-tumor lung tissues. P<0.05 and fold-change >1.5 or <0.67 was considered as significant. (C) GO analysis and functional annotation of differentially expressed proteins. GO, Gene Ontology; LUAD, lung adenocarcinoma.

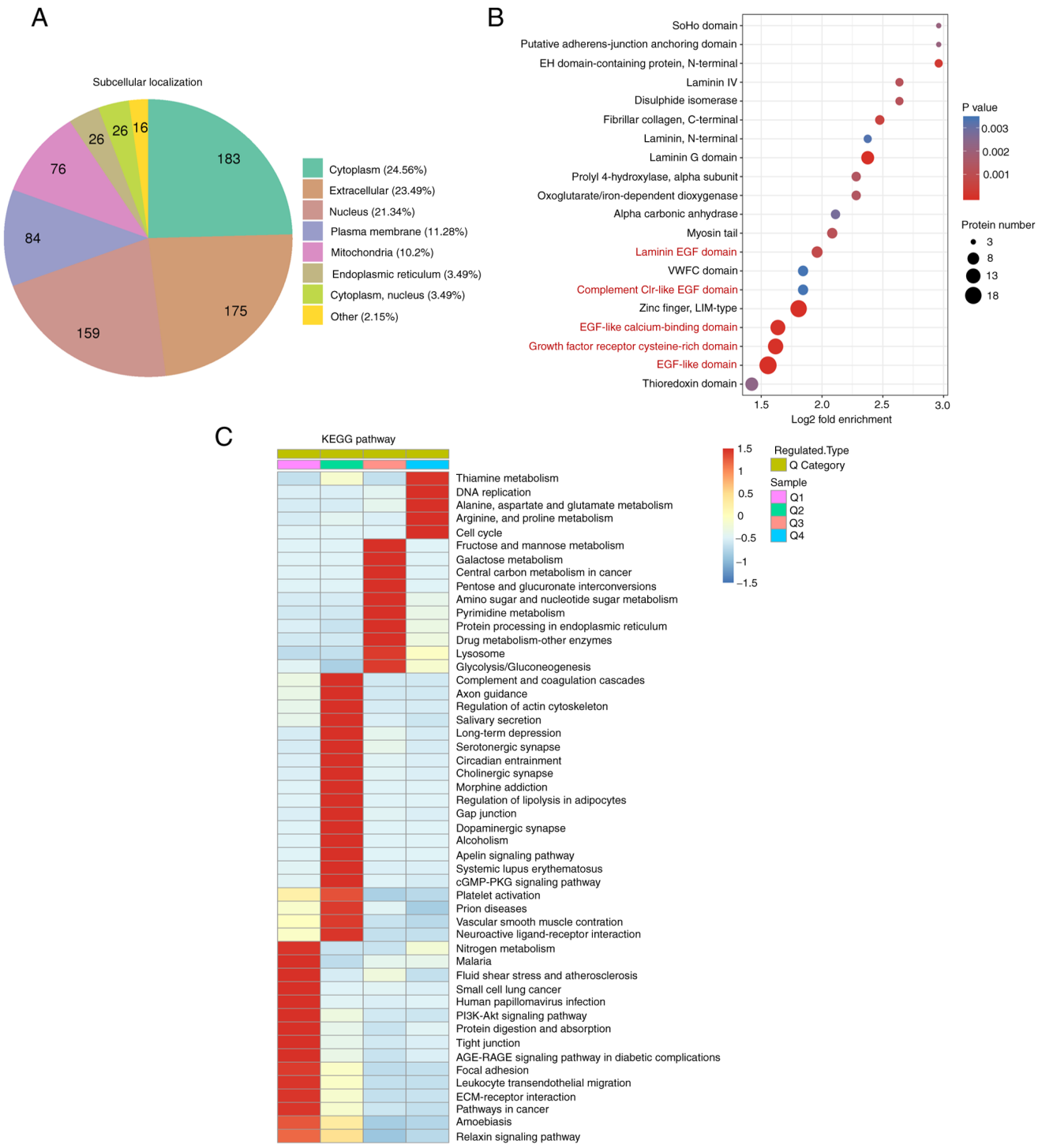

Figure 3. Subcellular location, protein domains and KEGG enrichment analysis of differentially expressed proteins in LUAD. (A) Percentage of differentially expressed proteins that localize to different subcellular locations. (B) Protein domain analysis of differentially expressed proteins in LUAD. Colored circles relate to P-value, where red represents significant enrichment of differentially expressed proteins (P<0.01). Circle size represents protein number. (C) KEGG enrichment analysis of differentially expressed proteins in LUAD. Proteins were classified into 4 categories: Q1<0.5, 0.5<Q2<0.67, 1.5<Q3<2 and Q4>2. Scale bar ranging from -1.5 to 1.5 is -$\log_{10}$ P-value. KEGG, Kyoto Encyclopedia of Genes and Genomes; LUAD, lung adenocarcinoma; Q, T/NT ratio.

CC, the upregulated proteins in cancer tissues were mostly enriched in 'endoplasmic reticulum (ER) lumen', while the downregulated proteins mostly focused on 'extracellular space', 'proteinaceous extracellular matrix' and 'extracellular region' (Fig. 4A). A large number of upregulated ER and Golgi proteins indicated that protein synthesis and amino acid metabolism were accelerated in patients with LUAD, and the large-scale downregulation of extracellular matrix proteins may be associated with the low production of extracellular mucus. In MF, the most highly expressed proteins were associated with 'isomerase activity' and 'procollagen-proline dioxygenase activity', and most of the low-expression proteins were associated with 'structural molecule activity' and 'actin binding' (Fig. 4B). In BP, high-expression proteins were mostly associated with metabolism, while low-expression proteins were mainly enriched in multicellular processes and cell

Table III. Differentially expressed membrane proteins in LUAD tissues and matched-adjacent nontumor tissues.

Protein accession	Gene name	T/NT Ratio	Regulation type	T/NT P-value
P53985	SLC16A1	2.272	Up	0.021444
P50281	MMP14	1.944	Up	0.010844
O15427	SLC16A3	1.823	Up	0.010179
P53634	CTSC	1.798	Up	0.009536
Q07812	BAX	1.732	Up	0.000204
O15260	SURF4	1.619	Up	0.002158
O96005	CLPTM1	1.589	Up	0.006359
Q03519	TAP2	1.553	Up	0.018917
Q8IWA5	SLC44A2	0.568	Down	0.000458
P08473	MME	0.553	Down	0.003921
P56199	ITGA1	0.541	Down	0.000276
P04003	C4BPA	0.53	Down	0.003395
P07204	THBD	0.517	Down	0.000996
P98172	EFNB1	0.486	Down	0.00156
P08514	ITGA2B	0.48	Down	0.007982
P56856	CLDN18	0.463	Down	0.019284
P04921	GYPC	0.367	Down	0.000904
P16671	CD36	0.338	Down	0.007999

adhesion (Fig. 4C). The upregulation of metabolic processes was consistent with most features of cancer.

Protein biomarker validation and overview of kinases and post-translational modification enzymes in LUAD. Cancer cells require profound remodeling of cellular metabolism to meet the energy requirements for aerobic glycolysis rather than mitochondrial oxidative phosphorylation (even under aerobic conditions), a common phenomenon known as the Warburg effect. In the present study, the expression of hexokinase 2, an important rate-limiting enzyme in aerobic glycolysis, was upregulated in cancer tissues (Fig. 5A). Moreover, the expression of some other important enzymes in aerobic glycolysis was also upregulated in cancer tissues (Fig. 5A).

Effective biomarkers are essential to improving diagnosis and treatment in a number of human diseases, including cancer, and some proteins were reported as biomarkers of LUAD in a previous proteomics study (4,15), the results of which are consistent with those of the present study. As shown in Fig. 5B, the expression of macrophage migration inhibitory factor and cofilin-1 was upregulated, while the expression of methanethiol oxidase, transgelin, annexin A1, A2 and A3 was downregulated in LUAD.

Post-translational modification (PTM) of proteins plays a vital role in the signaling networks of cancer and the regulation of cellular processes, including proliferation, cellular localization of proteins, and protein complex formation (16). Protein kinases, the key regulators of cellular function, not only regulate the process of phosphorylation, but are themselves regulated by phosphorylation and dephosphorylation processes (17). In the present study, enrichment analysis results showed that the expression levels of some kinases significantly changed across all eight samples. For example, the expression of adenylate kinase 4 and phosphofructokinase platelet were upregulated in cancer tissues (Fig. 5C). For ubiquitination regulatory proteins, the expression of E3 ubiquitin-protein ligase ring finger protein 213 (RNF213) was upregulated, while the expression of E3 ubiquitin-protein ligase RNF123 was downregulated in LUAD. In addition, the expression of F-box only protein 7 was increased in LUAD. For methylation, the expression of recombinant myosin light chain kinase was downregulated in LUAD, suggesting that kinases and PTM of proteins plays a significant role in LUAD.

ATAD3a expression is upregulated in LUAD. Proteomics analysis revealed that ATAD3a was more highly expressed in LUAD than in adjacent nontumor tissues (Fig. 6A). To verify the accuracy of the proteomics analysis, immunohistochemical analysis of ATAD3a expression was performed using FFPE tissue sections. The results showed that ATAD3a expression was significantly higher in cancer tissues than in adjacent nontumor lung tissues (Fig. 6B), which is consistent with the results of the proteomics analysis. Western blot results also showed that ATAD3a expression was significantly higher in LUAD cancer cell lines (A549 and NCI-H292) than in immortalized normal alveolar epithelial cells (HPAEpi C) (Fig. 6C and D).

ATAD3a downregulation enhances the sensitivity of LUAD cells to cisplatin by regulating cellular proliferation, the cell cycle and apoptosis. To study the effects of ATAD3a expression on the sensitivity of NCI-H292 cells to cisplatin, si-ATAD3a was used to knockdown expression. RT-qPCR and western blot analyses showed that ATAD3a mRNA and protein expression were significantly downregulated in NCI-H292 cells transfected with si-ATAD3a, compared with the control and si-NC

Table IV. Differentially expressed EGF domain-related proteins in LUAD tissues and matched-adjacent nontumor tissues.

Domain description	Gene name	T/NT ratio	Regulation type
Laminin EGF domain	CRELD2	1.86	Up
Laminin EGF domain	LAMA3	0.4	Down
Laminin EGF domain	HSPG2	0.5	Down
Laminin EGF domain	LAMB2	0.39	Down
Laminin EGF domain	LAMC1	0.41	Down
Laminin EGF domain	LAMA5	0.41	Down
Laminin EGF domain	AGRN	0.6	Down
EGF-like domain, extracellular	TNC	1.94	Up
EGF-like domain, extracellular	TNXB	0.54	Down
EGF-like domain	FBLN5	0.48	Down
EGF-like domain	LTBP4	0.54	Down
EGF-like domain	CRELD2	1.86	Up
EGF-like domain	LAMA3	0.4	Down
EGF-like domain	LTBP2	0.66	Down
EGF-like domain	NID2	0.58	Down
EGF-like domain	EFEMP1	0.55	Down
EGF-like domain	HSPG2	0.5	Down
EGF-like domain	FBLN2	0.65	Down
EGF-like domain	LAMB2	0.39	Down
EGF-like domain	THBS2	3.19	Up
EGF-like domain	TNC	1.94	Up
EGF-like domain	TNXB	0.54	Down
EGF-like domain	NID1	0.41	Down
EGF-like domain	LAMC1	0.41	Down
EGF-like domain	THBD	0.52	Down
EGF-like domain	LDLR	0.64	Down
EGF-like domain	F9	0.58	Down
EGF-like domain	LAMA5	0.41	Down
EGF-like domain	AGRN	0.6	Down
EGF-like calcium-binding domain	FBLN5	0.48	Down
EGF-like calcium-binding domain	LTBP4	0.54	Down
EGF-like calcium-binding domain	CRELD2	1.86	Up
EGF-like calcium-binding domain	LTBP2	0.66	Down
EGF-like calcium-binding domain	NID2	0.58	Down
EGF-like calcium-binding domain	EFEMP1	0.55	Down
EGF-like calcium-binding domain	HSPG2	0.5	Down
EGF-like calcium-binding domain	FBLN2	0.65	Down
EGF-like calcium-binding domain	THBS2	3.19	Up
EGF-like calcium-binding domain	NID1	0.41	Down
EGF-like calcium-binding domain	THBD	0.52	Down
EGF-like calcium-binding domain	F9	0.58	Down
EGF-like calcium-binding domain	AGRN	0.6	Down
EGF domain	NID2	0.58	Down
EGF domain	THBS2	3.19	Up
EGF domain	NID1	0.41	Down

groups (Fig. 7A and B). As predicted, colony formation assays demonstrated that si-ATAD3a increased cisplatin-induced growth inhibition in NCI-H292 cells (Fig. 7C). Flow cytometry revealed that si-ATAD3a increased cisplatin-induced G_1-stage arrest and apoptosis in NCI-H292 cells (Fig. 7D and E). These data indicated that knocking down ATAD3a enhanced the sensitivity of NCI-H292 cells to cisplatin by regulating proliferation, the cell cycle and apoptosis.

Figure 4. Gene Ontology functional classification analysis of all differentially expressed proteins. (A) Cellular component, (B) molecular function and (C) biological process. The different expressed proteins were classified into 4 categories: Q1<0.5, 0.5<Q2<0.67, 1.5<Q3<2 and Q4>2. Scale bar ranging from -1.5 to 1.5 is $-\log_{10}$ P-value.

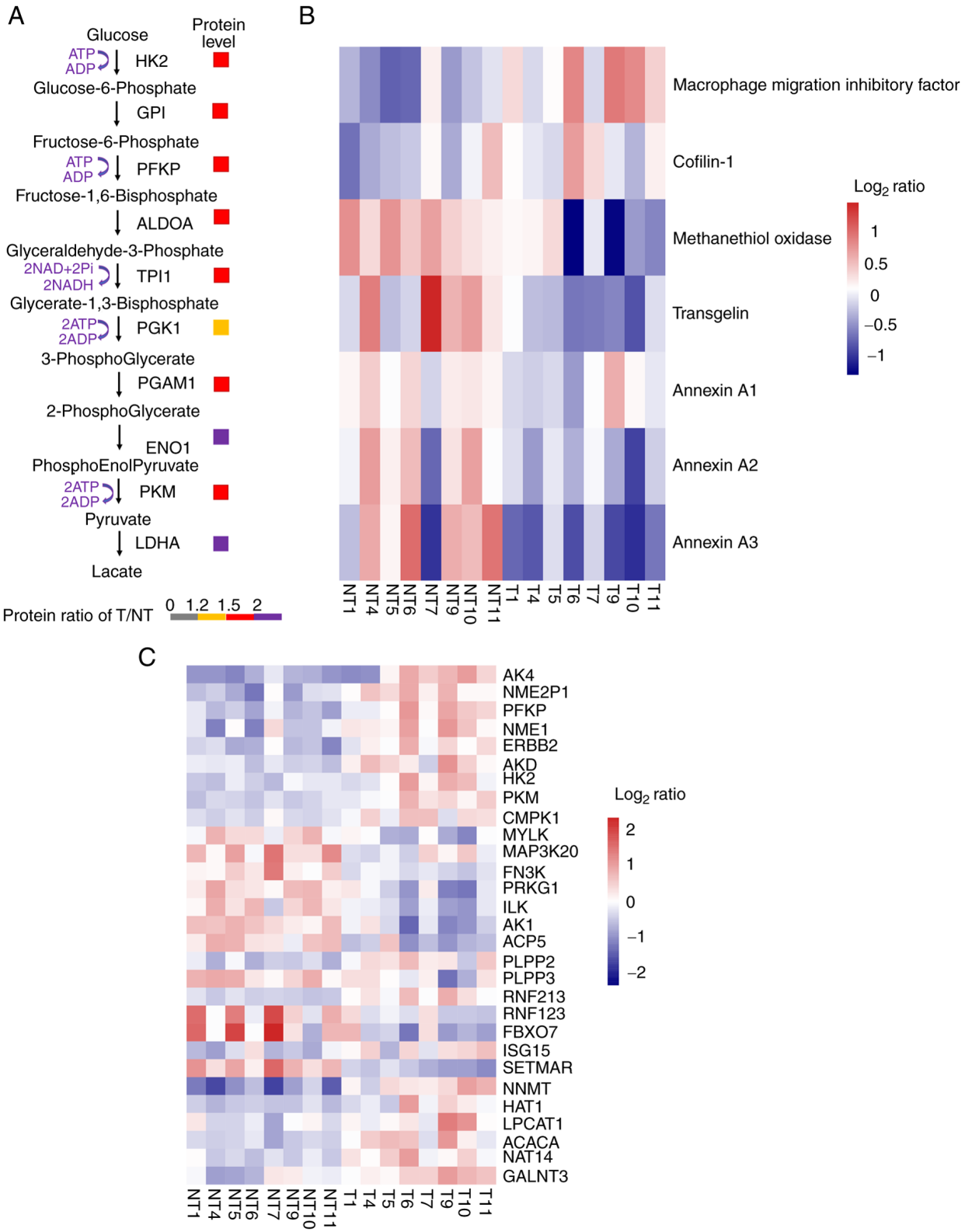

Figure 5. Protein biomarker validation, overview of kinases and post-translational modification enzymes in lung adenocarcinoma. (A) Fold-change between tumor and corresponding normal tissues. (B and C) Level of change of T/NT (i.e., either increase or decrease) in protein expression was determined as: i) Low (-1≤$\log_2$ ratio<0); ii) medium ($\log_2$ ratio=0); or iii) high (0<$\log_2$ ratio≤1.0). (HK2, hexokinase 2; GPI, glucose 6 phosphate isomerase; PFKP, phosphofructokinase; ALDOA, fructose-bisphosphate aldolase A; TPI1, triosephosphate isomerase 1; PGK1, phosphoglycerate kinase 1; PGAM1, phosphoglycerate mutase 1; ENO1, enolase 1α; PKM, pyruvate kinase M; LDHA, lactate dehydrogenase A; AK4, adenylate kinase 4; NME2P, non-metastatic2 pseudogene 1; PFKP, phosphofructokinase, platelet; NME1, non-metastatic cells 1; ERBB2, V-erb-b2 erythroblastic leukemia viral oncogene homolog 2; ADK, adenylate kinase; CMPK1, cytidine monophosphate kinase 1; MYLK, myosin light chain kinase; MAP3K20, mitogen-activated protein kinase kinase kinase 20; FN3K, fructosamine-3-kinase; PRKG1, protein kinase, cGMP dependent type I; ILK, integrin-1inked kinase; AK1, adenylate kinase 1; ACP5, acid phosphatase 5 tartrate resistant; PLPP2/3, phospholipid phosphatase 2/3; RNF213/123, E3 ubiquitin-protein ligase RNF213/123; FBXO7, F-box only protein 7; ISG15, interferon-stimulated gene 15; SETMAR, SET domain and mariner transposase fusion gene; NNMT, nicotinamide N-methyltransferase; HAT1, histone acetyltransferase 1; LPCAT1, lysophos-phatidylcholineacyltransferase 1; ACACA, acetylcoenzyme A carboxylase α; NAT14, N-acetyltransferase 14; GALNT3, polypeptide N-acetylgala-ctosaminyltransferase 3.

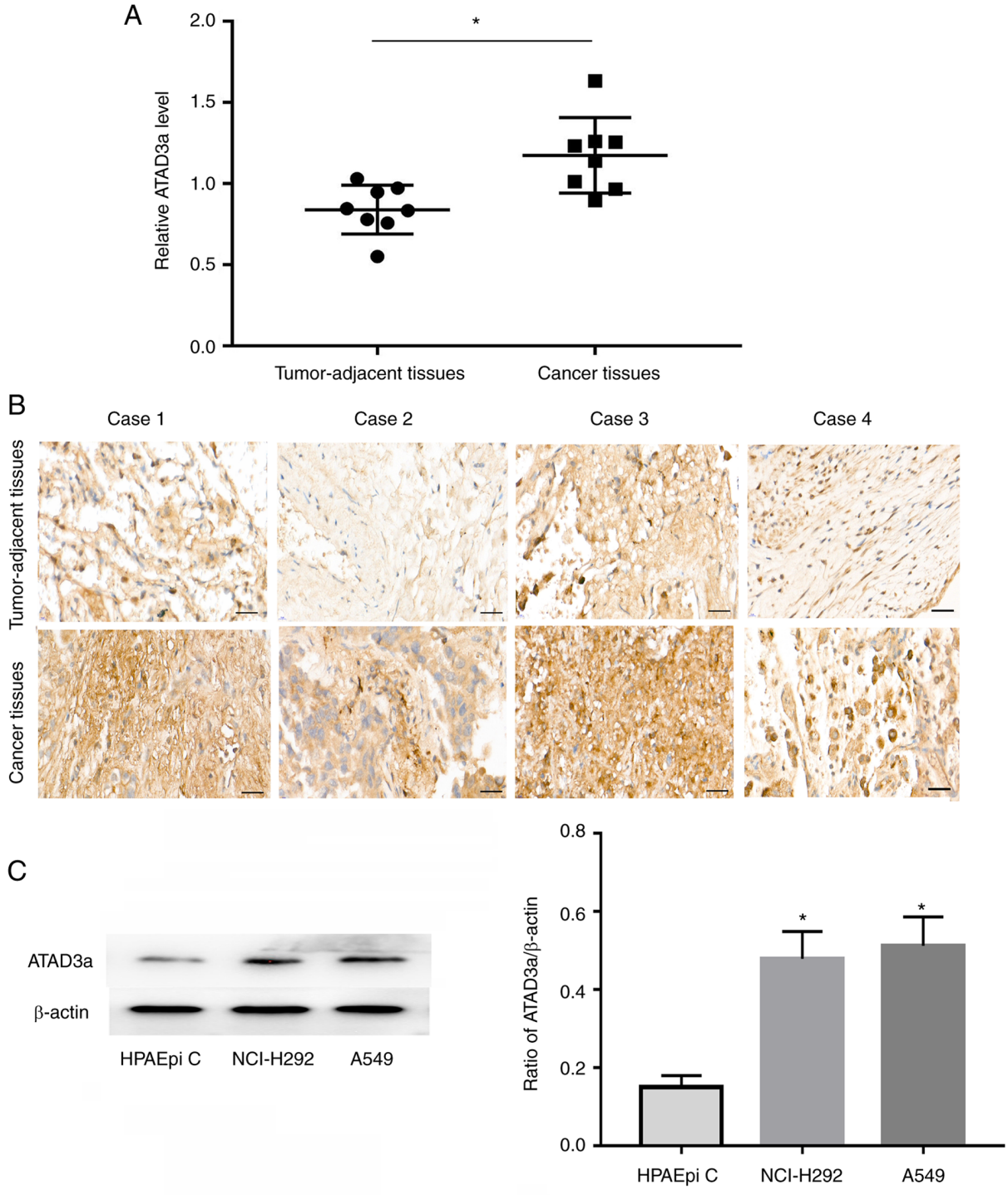

Figure 6. ATAD3a expression is upregulated in LUAD. (A) Expression of ATAD3a in seven pairs of formalin-fixed, paraffin-embedded LUAD tissues and tumor-adjacent tissues was detected by proteomics. *P<0.05. (B) Representative images of ATAD3a immunohistochemical staining in LUAD samples; scale bar, 30 μm. (C) Western blot analysis to examine protein expression levels of ATAD3a in HPAEpiC, NCI-H292 and A549 cells. *P<0.05 vs. HPAEpiC cells. LUAD, lung adenocarcinoma; ATAD3a, AAA domain containing 3A.

Discussion

Lung cancer remains the leading cause of cancer-related deaths among women and men worldwide. Moreover, <15% of patients survive for 5 years following diagnosis at the advanced stages of disease (1,18). Lung cancer is categorized as NSCLC and SCLC based on histological characteristics. NSCLC, which accounts for ~85% of all lung cancers, can be further divided into two major histological subtypes, LUAD and LUSC (19). LUAD is found in 60% of this population. Despite efforts to improve effective treatment, the prognosis of LUAD remains poor due to the lack of specific biomarkers and personalized medical regimes (3).

Proteomics not only gains insights into the overall landscape of proteome-wide alterations of post-translational modifications and signaling pathways, but also offers information on

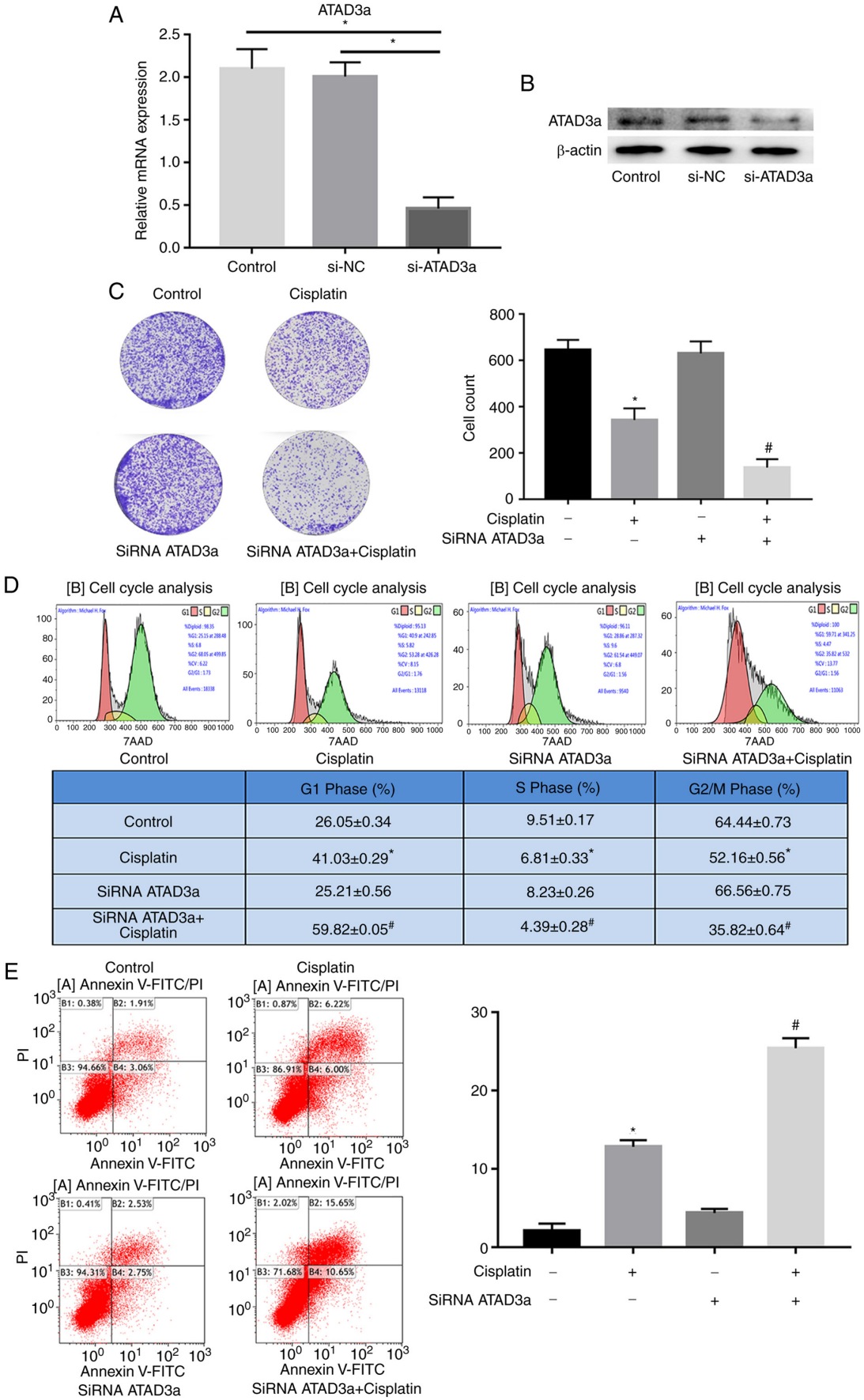

	G1 Phase (%)	S Phase (%)	G2/M Phase (%)
Control	26.05±0.34	9.51±0.17	64.44±0.73
Cisplatin	41.03±0.29*	6.81±0.33*	52.16±0.56*
SiRNA ATAD3a	25.21±0.56	8.23±0.26	66.56±0.75
SiRNA ATAD3a+ Cisplatin	59.82±0.05#	4.39±0.28#	35.82±0.64#

Figure 7. ATAD3a downregulation enhances lung adenocarcinoma cell sensitivity to cisplatin by regulating proliferation, the cell cycle and apoptosis. (A) Reverse transcription-quantitative PCR and (B) western blot analysis were used to detect the expression levels of ATAD3a mRNA and protein, respectively. *P<0.05. (C) Colony formation assays were used to evaluate the proliferation ability of NCI-H292 cells treated with 10 μg/ml cisplatin and/or siRNA ATAD3a. *P<0.05 vs. control, #P<0.05 vs. cisplatin. (D) Cell cycle distribution and (E) apoptotic levels of NCI-H292 cells treated with 10 μg/ml cisplatin and/or siRNA ATAD3a was detected by flow cytometry. *P<0.05 vs. control. #P<0.05 vs. cisplatin. ATAD3a, AAA domain containing 3A; si, small interfering.

protein-protein interactions and the associated underlying mechanisms (20). FFPE tissue samples offer comprehensive information for clinical and biomarker research, and have been shown to be a rich resource for clinical research and the most widely available tissue preservation method (21,22). Using high-throughput proteomics analysis, Zhu *et al* (22) confirmed that FFPE tissue samples had great potential for the identification of novel, promising protein biomarkers for prostate carcinoma (22). In the present study, FFPE LUAD and adjacent-nontumor lung tissues were selected for proteomics analysis.

Immunotherapy can promote the anticancer properties of the immune system, and hence plays an important role in LUAD treatment (23-25). Compared with cytotoxic chemotherapy, immunotherapy has a unique toxicity profile and the ability to provide prolonged clinical benefit for patients (24). Marinelli *et al* (26) confirmed that the efficacy of immunotherapy had notable interpatient heterogeneity in patients with LUAD. In addition, immune checkpoint inhibitors were of benefit to a great deal patients with LUAD, and a small mutation panel of coding sequences could predict the long-term outcome of immunotherapy (27). In the current study, 19 differentially expressed membrane proteins were found to be associated with immune processes, indicating that these cell membrane proteins may be potential immunotherapeutic targets. The subcellular location patterns of proteins provided crucial information for understanding the underlying mechanism and functions of specific proteins, which varied across different pathological types and cellular conditions (28). In the present study, the most differentially expressed proteins were localized to the cytoplasm, followed by the extracellular matrix, nucleus and plasma membrane.

A large number of recent studies have shown that protein domains serve a vital role in tumorigenesis and progression (29-32). Numerous proteins comprise more than one domain, and each domain, a stable unit of the protein structure, is responsible for a particular molecular function. In the present study, 'EGF-like calcium-binding domain', 'EGF-like domain' and 'laminin EGF domain' showed considerable differential expression levels between LUAD and adjacent-nontumor lung tissues (33). EGF is a growth factor that stimulates cellular proliferation and differentiation (30). EGF binds to the extracellular domain of EGFR and induces its dimerization, activating its intrinsic kinase activity (34,35). EGF/EGFR signaling has been recognized as an important molecular target in cancer therapy. The tyrosine kinase inhibitors (TKIs) of EGFR are regarded as the first-line standard option for patients with LUAD with EGFR mutations, and EGFR mutation status determines the effectiveness of cancer therapies. Liang *et al* (36) confirmed that the EGFR mutation p.T790M was the most prominent resistance mechanism to TKI therapy in LUAD. Moreover, they also confirmed that after acquiring afatinib resistance, the p.T790M mutation could not occur in patients with LUAD who also possessed EGFR p.L747P or p.L747S mutations (36). In follow-up studies, further *in vivo* and *in vitro* experiments are required to explore the function or purpose of EGF-related domains and EGF-EGFR signaling in LUAD.

The basic characteristics of cancer cells primarily include strong proliferative capacity, high mutation rates and changes in metabolic pathways. Cancer cells have longer telomerases than normal cells, which are always in an active state, and allow cancer cells to continuously divide (37-39). Through KEGG analysis, pathways involved in cellular proliferation and DNA replication were found to be highly expressed in LUAD cancer tissues. Cancer is also a metabolic disease characterized by metabolic reprogramming to support rapid cellular proliferation. Ni *et al* (40) indicated that LUAD cells favored the Warburg effect even under oxygen-rich conditions, and that the metabolism of fatty acids and amino acids was associated with the occurrence and progression of cancer (40). In the present study, changes in some of the most important metabolic pathways, such as thiamine, alanine, aspartate and glutamate metabolism, occurred in patients with LUAD.

Cluster analysis of GO functional enrichment revealed that significantly upregulated proteins were primarily associated with 'ER lumen', 'protein disulfide isomerase activity', 'vitamin binding' and 'cell cycle G_1/S phase transition'. These results suggested that compared with paracancerous tissues, the abnormal expression of multiple proteins was related to 'response', 'binding' or 'activity' in LUAD. These findings broaden the current understanding of LUAD. Tumor biomarkers are defined as molecular or process-based changes that reflect the status of an underlying malignancy. They can be divided into three categories: i) Diagnostic biomarkers, (monitoring of asymptomatic individuals and detection of early-stage cancer); ii) prognostic biomarkers (predicting disease outcome and monitoring disease recurrence); and iii) predictive biomarkers (monitoring sensitivity to therapy and therapy response and aiding treatment decisions) (41-43).

PTM enzymes perform >200 types of post-translational modifications, including acetylation, ubiquitination, phosphorylation, nitrosylation and methylation (44), and affect nearly all aspects of cancer biology and pathogenesis. A number of studies have confirmed that PTMs may serve as biomarkers of cancer (44). The present study not only validated seven LUAD-specific biomarkers by enrichment analysis, but also found that the expression of numerous kinases and PTM enzymes was significantly upregulated across all eight LUAD samples compared with paracarcinoma tissues, suggesting that these proteins had the potential to be novel biomarkers and may be beneficial to the development of personalized treatments plans. Because the early symptoms of LUAD are not apparent in the early stages of disease, 50-60% of LUAD is confirmed at the advanced stage. Cisplatin is the most commonly used platinum-based drug, and plays an important role in advanced LUAD. Patients are susceptible to cisplatin in early treatment. However, resistance to LUAD has become a key obstacle in the effective treatment of patients. ATAD3a, an integral mitochondrial membrane protein, has been reported to be closely associated with cancer cell metabolism, proliferation, apoptosis and chemotherapy (45). Therefore, the present study aimed to explore the role and mechanism of ATAD3a in LUAD. ATAD3a expression was measured by immunohistochemical and western blot analyses, and the results were in accordance with those of the proteomics data analysis. The study also confirmed that ATAD3a downregulation enhanced the sensitivity of LUAD cells to cisplatin by regulating cellular proliferation, the cell cycle and apoptosis. However, the specific molecular mechanisms underlying ATAD3a upregulation in

LUAD remain unknown. Hence, further studies should be conducted to determine the potential involvement of ATAD3a in LUAD. To conclude, the results of the present study provided an improved understanding of potential therapeutic targets for patients with LUAD.

Acknowledgements

The authors would like to thank Mr. Bin Wang (M.S. Sales Representative at PTM Biolabs, Inc. Hangzhou, China) for TMT labeling, HPLC fractionation and LC-MS/MS analysis.

Funding

The present study was supported by grants from the Major Project of Science and Technology in Henan province (grant no. 161100311400), the Medical Science and Technique Foundation of Henan Provincial and ministry co-construction project (grant no. SB201901084), and the Scientific Research Staring Foundation for doctor of Henan Provincial People's Hospital (grant no. 201701).

Availability of data and materials

The datasets used and/or analyzed during the current study are available from the corresponding author on reasonable request.

Authors' contributions

QX performed most of the experiments and drafted the initial manuscript. QX, ZL and LK were responsible for the study conception and design. DW, XL and AH performed the experiments, and analyzed and interpreted the data. HY, JT and PG performed statistical and computational analyses. TS analyzed the data and carried out the literature research. TS and LK supervised the study, acquired funding, collected the tissues and edited the manuscript. LK and TS confirmed the authenticity of the data. All authors have read and approved the final manuscript.

Ethics approval and consent to participate

The present study was approved by the Research Ethics Committee of Henan Provincial People's Hospital (Zhengzhou, China; approval no. 2019-050) and written informed consent was provided by all patients prior to the study start.

Patient consent for publication

Not applicable.

Competing interests

The authors declare that they have no competing interests.

References

1. Bezzecchi E, Ronzio M, Semeghini V, Andrioletti V, Mantovani R and Dolfini D: NF-YA overexpression in lung cancer: LUAD. Genes (Basel) 11: 198, 2020.
2. Xu M, Wang D, Wang X and Zhang Y: Correlation between mucin biology and tumor heterogeneity in lung cancer. Semin Cell Dev Biol 64: 73-78, 2017.
3. Haragan A, Field JK, Davies MPA, Escriu C, Gruver A and Gosney JR: Heterogeneity of PD-L1 expression in non-small cell lung cancer: Implications for specimen sampling in predicting treatment response. Lung Cancer 134: 79-84, 2019.
4. Böttge F, Schaaij-Visser TB, de Reus I, Piersma SR, Pham T, Nagel R, Brakenhoff RH, Thunnissen E, Smit EF and Jimenez CR: Proteome analysis of non-small cell lung cancer cell line secretomes and patient sputum reveals biofluid biomarker candidates for cisplatin response prediction. J Proteomics 196: 106-119, 2019.
5. Wang Y, Tian M, Chang Y, Xue C and Li Z: Investigation of structural proteins in sea cucumber (*Apostichopus japonicus*) body wall. Sci Rep 10: 18744, 2020.
6. Bradshaw RA, Hondermarck H and Rodriguez H: Cancer proteomics and the elusive diagnostic biomarkers. Proteomics 19: e1800445, 2019.
7. Wang C, Yang S, Jin L, Dai G, Yao Q, Xiang H, Zhang Y, Liu X and Xue B: Biological and clinical significance of GATA3 detected from TCGA database and FFPE sample in bladder cancer patients. Onco Targets Ther 13: 945-958, 2020.
8. Zhong J, Ye Z, Clark CR, Lenz SW, Nguyen JH, Yan H, Robertson KD, Farrugia G, Zhang Z, Ordog T and Lee JH: Enhanced and controlled chromatin extraction from FFPE tissues and the application to ChIP-seq. BMC Genomics 20: 249, 2019.
9. Greytak SR, Engel KB, Bass BP and Moore HM: Accuracy of molecular data generated with FFPE biospecimens: Lessons from the Literature. Cancer Res 75: 1541-157, 2015.
10. Zakrzewski F, Gieldon L, Rump A, Seifert M, Grützmann K, Krüger A, Loos S, Zeugner S, Hackmann K, Porrmann J, *et al*: Targeted capture-based NGS is superior to multiplex PCR-based NGS for hereditary BRCA1 and BRCA2 gene analysis in FFPE tumor samples. BMC Cancer 19: 396, 2019.
11. Coscia F, Doll S, Bech JM, Schweize L, Mund A, Lengyel E, Lindebjerg J, Madsen GI, Moreira JM and Mann M: A streamlined mass spectrometry-based proteomics workflow for large-scale FFPE tissue analysis. J Pathol 251: 100-112, 2020.
12. Marchione DM, Ilieva I, Devins K, Sharpe D, Pappin DJ, Garcia BA, Wilson JP and Wojcik JB: HYPERsol: High-quality data from archival FFPE tissue for clinical proteomics. J Proteome Res 19: 973-983, 2020.
13. Lang L, Loveless R and Teng Y: Emerging links between control of mitochondrial protein ATAD3A and cancer. Int J Mol Sci 21: 7917, 2020.
14. Slizen MV and Galzitskaya OV: Comparative analysis of proteomes of a number of nosocomial pathogens by KEGG modules and KEGG pathways. Int J Mol Sci 21: 7839, 2020.
15. Camidge DR, Doebele RC and Kerr KM: Comparing and contrasting predictive biomarkers for immunotherapy and targeted therapy of NSCLC. Nat Rev Clin Oncol 16: 341-355, 2019.
16. Han Z, Feng Y, Gu B, Li Y and Chen H: The post-translational modification, SUMOylation, and cancer (Review). Int J Oncol 52: 1081-1094, 2018.
17. Lu Z and Hunter T: Metabolic kinases moonlighting as protein kinases. Trends Biochem Sci 43: 301-310, 2018.
18. Barton MK: Structured palliative care program found to be helpful for caregivers of patients with lung cancer. CA Cancer J Clin 66: 5-6, 2016.
19. Xu J, Zhang C, Wang X, Zhai L, Ma Y, Mao Y, Qian K, Sun C, Liu Z, Jiang S, *et al*: Integrative proteomic characterization of human lung adenocarcinoma. Cell 182: 245-261.e17, 2020.
20. Keskin O, Tuncbag N and Gursoy A: Predicting protein-protein interactions from the molecular to the proteome level. Chem Rev 116: 4884-4909, 2016.
21. Newton Y, Sedgewick AJ, Cisneros L, Golovato J, Johnson M, Szeto CW, Rabizadeh S, Sanborn JZ, Benz SC and Vaske C: Large scale, robust, and accurate whole transcriptome profiling from clinical formalin-fixed paraffin-embedded samples. Sci Rep 10: 17597, 2020.
22. Zhu Y, Weiss T, Zhang Q, Sun R, Wang B, Yi X, Wu Z, Gao H, Cai X, Ruan G, *et al*: High-throughput proteomic analysis of FFPE tissue samples facilitates tumor stratification. Mol Oncol 13: 2305-2328, 2019.
23. Park C, Na KJ, Choi H, Ock CY, Ha S, Kim M, Park S, Keam B, Kim TM, Paeng JC, *et al*: Tumor immune profiles noninvasively estimated by FDG PET with deep learning correlate with immunotherapy response in lung adenocarcinoma. Theranostics 10: 10838-10848, 2020.

24. Xu F, Zhan X, Zheng X, Xu H, Li Y, Huang X, Lin L and Chen Y: A signature of immune-related gene pairs predicts oncologic outcomes and response to immunotherapy in lung adenocarcinoma. Genomics 112: 4675-4683, 2020.
25. Li Y, Jiang W, Li T, Li M, Li X, Zhang Z, Zhang S, Liu Y, Zhao W, Gu Y, *et al*: Identification of a small mutation panel of coding sequences to predict the efficacy of immunotherapy for lung adenocarcinoma. J Transl Med 18: 25, 2020.
26. Marinelli D, Mazzotta M, Scalera S, Terrenato I, Sperati F, D'Ambrosio L, Pallocca M, Corleone G, Krasniqi E, Pizzuti L, *et al*: KEAP1-driven co-mutations in lung adenocarcinoma unresponsive to immunotherapy despite high tumor mutational burden. Ann Oncol 12: 1746-1754, 2020.
27. Wu C and Hwang MJ: Risk stratification for lung adenocarcinoma on EGFR and TP53 mutation status, chemotherapy, and PD-L1 immunotherapy. Cancer Med 8: 5850-5861, 2019.
28. Du P and Xu C: Predicting multisite protein subcellular locations: Progress and challenges. Expert Rev Proteomics 10: 227-237, 2013.
29. Laursen L, Karlsson E, Gianni S and Jemth P: Functional interplay between protein domains in a supramodular structure involving the postsynaptic density protein PSD-95. J Biol Chem 295: 1992-2000, 2020.
30. Dawson N, Sillitoe I, Marsden RL and Orengo CA: The classification of protein domains. Methods Mol Biol 1525: 137-164, 2017.
31. Zheng W, Zhou X, Wu Q, Pearce R, Li Y and Zhang Y: FUpred: Detecting protein domains through deep-learning-based contact map prediction. Bioinformatics 12: 3749-3757, 2020.
32. Libiad M, Motl N, Akey DL, Sakamoto N, Fearon ER, Smith JL and Banerjee R: Thiosulfate sulfurtransferase-like domain-containing 1 protein interacts with thioredoxin. J Biol Chem 293: 2675-2686, 2018.
33. Lu Y, Mehta-D'souza P, Biswas I, Villoutreix BO, Wang X, Ding Q and Rezaie AR: Ile73Asn mutation in protein C introduces a new N-linked glycosylation site on the first EGF-domain of protein C and causes thrombosis. Haematologica 105: 1712-1722, 2020.
34. Wang F, Wang-Gou S, Cao H, Jiang N and Li X: Proteomics identifies EGF-like domain multiple 7 as a potential therapeutic target for epidermal growth factor receptor-positive glioma. Cancer Commun (Lond) 40: 518-530, 2020.
35. Mizutani K, Guo X, Shioya A, Zhang J, Zheng J, Kurose N, Ishibashi H, Motono N, Uramoto H and Yamada S: The impact of PRDX4 and the EGFR mutation status on cellular proliferation in lung adenocarcinoma. Int J Med Sci 16: 1199-1206, 2019.
36. Liang S, Ko JC, Yang J and Shih JY: Afatinib is effective in the treatment of lung adenocarcinoma with uncommon EGFR p.L747P and p.L747S mutations. Lung Cancer 133: 103-109, 2019.
37. Neugut AI, MacLean SA, Dai W and Jacobson JS: Physician characteristics and decisions regarding cancer screening: A systematic review. Popul Health Manag 22: 48-62, 2019.
38. Heldring N, Nyman U, Lönnerberg P, Onnestam S, Herland A, Holmberg J and Hermanson O: NCoR controls glioblastoma tumor cell characteristics. Neuro Oncol 16: 241-249, 2014.
39. Wang H, Gao J, Zhang R, Li M, Peng Z and Wang H: Molecular and immune characteristics for lung adenocarcinoma patients with CMTM6 overexpression. Int Immunopharmacol 83: 106478, 2020.
40. Ni K, Wang D, Xu H, Mei F, Wu C, Liu Z and Zhou B: miR-21 promotes non-small cell lung cancer cells growth by regulating fatty acid metabolism. Cancer Cell Int 19: 219, 2019.
41. Barton MK: Use of posttreatment imaging and biomarker testing for survivors of breast cancer. CA Cancer J Clin 66: 175-176, 2016.
42. VanderLaan PA, Rangachari D, Majid A, Parikh MS, Gangadharan SP, Kent MS, McDonald DC, Huberman MS, Kobayashi SS and Costa DB: Tumor biomarker testing in non-small-cell lung cancer: A decade of change. Lung Cancer 116: 90-95, 2018.
43. Wu Y, Jamal M, Xie T, Sun J, Song T, Yin Q, Li J, Pan S, Zeng X, Xie S and Zhang Q: Uridine-cytidine kinase 2 (UCK2): A potential diagnostic and prognostic biomarker for lung cancer. Cancer Sci 110: 2734-2747, 2019.
44. Gu B and Zhu WG: Surf the post-translational modification network of p53 regulation. Int J Biol Sci 8: 672-684, 2012.
45. Teng Y, Lang L and Shay C: ATAD3A on the path to cancer. Adv Exp Med Biol 1134: 259-269, 2019.